PHOTOMETRIC IMAGING SEQUENCES AND ANALYSIS AT THE MARS PATHFINDER LANDING SITE. J.R. Johnson[1], L. Soderblom[1], R. Kirk[1], L. Gaddis[1], R. Reid[2], P.H. Smith[2], M. Lemmon[2], D. Britt[2], N. Thomas[3], J. Bell[4], N.T. Bridges[5], R. Anderson[5], K. Herkenhoff[5], S.M. Murchie[6], A. Dummel[7], G. Arnold[7], P. Lampen[7], F. Trauthan[7] , [1]United States Geological Survey, Flagstaff, AZ (jjohnson@flagmail.wr.usgs.gov), [2]Lunar and Planetary Laboratory, University of Arizona, Tucson, [3]Max Planck Institute for Aeronomy, Kathenburg-Lindau, Germany, [4]Cornell University, Ithaca, New York, [5]Jet Propulsion Laboratory, Pasadena, CA, [6]Applied Physics Laboratory, Johns Hopkins University, Laurel, MD, [7]DLR, Institute of Planetary Exploration, Berlin, Germany.

Multispectral imaging sequences designed to provide reflectance measurements of selected rocks and soils over a wide range of phase angles were obtained by the IMP camera onboard the Mars Pathfinder lander. The observed spectral variations of rocks and soils under different illumination geometries can be used to model the photometric properties of these materials. This provides constraints on interpretations of reflectance spectra relevant to understanding more precisely the physical and mineralogical nature and distribution of soils, rock types, and dust coatings on rocks at the landing site [cf. **1,2,4**].

Data sets. The data sets consist of (1) three small "photometric spot" sub-framed (64x64 pixel) scenes located approximately north (near the rock "Shaggy"), south (near the "Mermaid Dune"), and west of the lander ("Photometry Flats"), (2) two image strips composed of three sub-framed (96x248 pixel) images each, located along the anti-sunrise and anti-sunset lines ("Photometric equator") extending from near the lander to near the horizon; and (3) full-image scenes of the rock "Yogi." The photometric spot images were obtained in six filters (443, [480 or 860], 531, 671, 752, and 967 nm) at five times of day (0700, 0830, 1200, 1530, and 1700 LST) covering phase angles from 20-150 degrees on Sols 38-39 and 21, respectively. The photometric equator images were obtained in three filters (443, 752, 968 nm) at 0800, 1200, 1600, and 1700 LST covering phase angles from ~0-155 degrees on Sol 27. The Yogi images were obtained in four filters (443, 531, 671, and 967 nm) at 0740, 1500, 1640 LST over Sols 55-56 and at 0900 LST on Sol 75.

Data reduction. Multispectral images were calibrated to I/F using on-board calibration targets [**3,8**]. Image cubes were constructed for each LST observation and spectra were extracted for regions of interest. Phase angles were calculated for the center of each image assuming a flat surface; phase angles for sampled soils and rocks were then estimated using these values. (Future analyses will use stereo models to improve the accuracy of local facet orientations for individual rock and soil surfaces.)

Observations. Phase functions extracted from these data exhibit dominantly increasing reflectance at lower phase angles, indicating a backscattering photometric function, consistent with the results from the Viking lander cameras [**1,2**]. However, forward scattering behavior does appear when phase angles are > 130 degrees in some of the anti-sunrise photometric equator data. Also, instances of specular reflection (incidence and emission angles nearly equal) cause irregularities in some of the phase curves and may exaggerate the opposition effect or forward scattering [cf. **2**].

Photometry. **Figure 1** shows phase functions obtained from the anti-sunrise photometric equator sequence for bright drift soil, soil disturbed by contact with the spacecraft airbags during landing, and a typcial rock (class "bright rock" in [**8**]). Results of preliminary efforts to model photometric functions and parameters using a Hapke scattering model [**6**] are shown in **Table 1**. The apparent wavelength-dependence of the opposition width (*h)* for both soils is not consistent with Hapke theory [**6**] and is likely due to the sparse number of available phase function points, especially at low phase near the opposition surge. The disturbed soil is also difficult to model because of the variability in I/F values at high phase angles due to a greater degree of local shadowing. However, modeling does result in a single-scattering albedo (*w*) for the bright drift of 0.92 at 752 and 968 nm, which is equivalent to that determined for atmospheric dust using Viking IRTM data [**5**]. This is consistent with the idea that bright drift material is composed at least partially of deposited airborne dust particles [**8].** The diagnostically "darker" disturbed soil [**8**] has a lower *w* and higher surface roughness (q–bar) than the bright drift, as expected. The rock has the same surface roughness as bright drift, with a *w* lower at 752 and 968 nm and higher at 440 nm, consistent with its "gray" reflectance relative to bright drift [**8,9**].

Future enhancement of IMP calibration methods [**3**] will refine the precision of these measurements and potentially improve our understanding of surface roughness, particle size distributions and coatings of materials at the landing site.

ACKNOWLEDGEMENTS. We thank D. Domingue (APL) for use of her disk-resolved Hapke model.

REFERENCES: [**1**] Arvidson et al., JGR, 94, 1573, 1989; [**2**] Guinness, E.A.,, *J. Geophys. Res*., 86, 7983-7992, 1981; Guinness et al., *J. Geophys. Res*., 92, E575-E587, 1987; Guinness et al., *J. Geophys. Res.*, 102, 28687-28703, 1997. [**3**] Reid et al., EOS. Trans. AGU, 78, 402, 1997; [**4**] Israel et al., *J. Geophys. Res*., 102, 28705-28716, 1997 [**5**] Clancy et al., *J. Geophys. Res*., 100, 5251-5263, 1995 [**6**] Domingue, D., and B. Hapke, *Icarus*, 99, 70-81, 1992; Domingue et al., *Icarus*, 128, 28-48, 1997 [**7**] Golombek et al., *Science*, 278, 1743-1748, 1997; [**8**] Smith et al., *J. Geophys. Res*., 102, 4003-4026, 1997; Smith et al., *Science*, 278, 1758-1765, 1997b; [**9**]

Murchie et al., EOS. Trans. AGU, 78, 396, 1997;Bell et al., EOS. Trans. AGU, 78, 396, 1997.

Figure 1. Phase functions extracted from the anti-sunrise "photometric equator" imaging sequence.

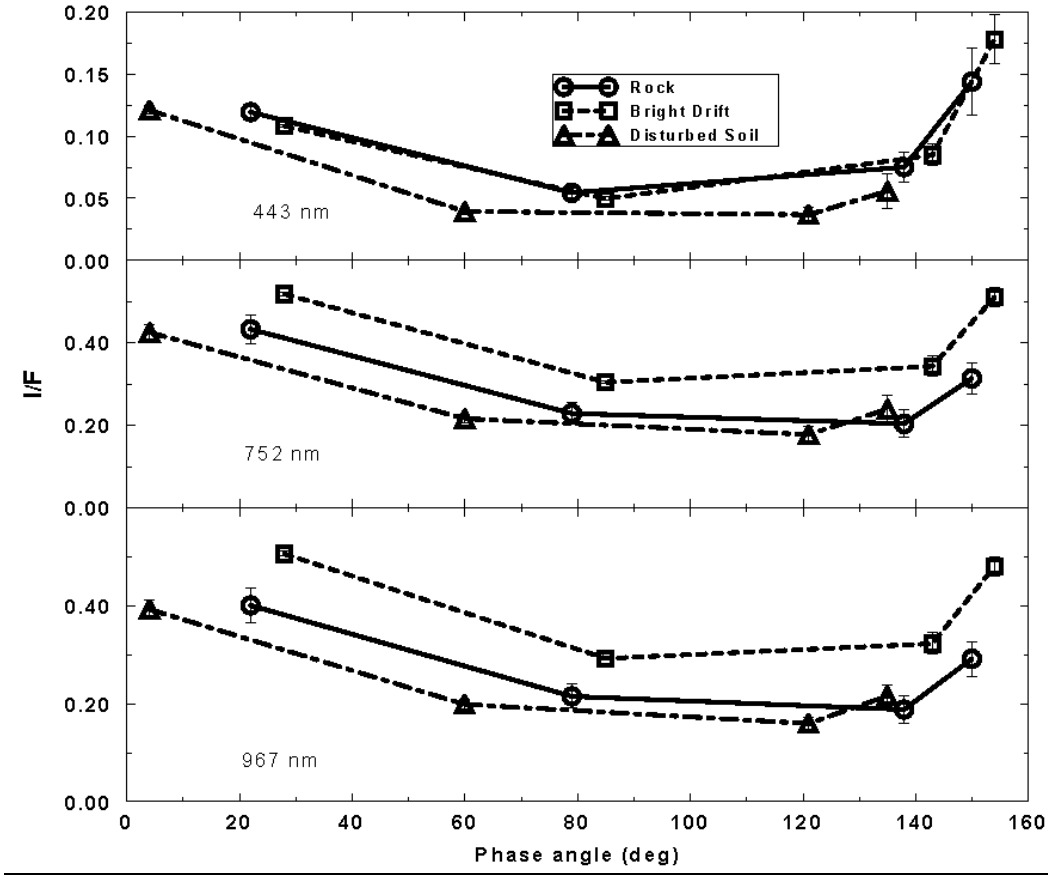

Table 1. Preliminary Hapke scattering model parameters from anti-sunrise "photometric equator."

	Bright Drift			*Disturbed Soil*			*Rock*		
Parameter	443 nm	750 nm	968 nm	443 nm	750 nm	968 nm	443 nm	752 nm	968 nm
w	0.50 ±0.03	0.92 ±0.03	0.92 ±0.03	0.44 ±0.03	0.81 ±0.03	0.78 ±0.03	0.54 ±0.03	0.88 ±0.03	0.86 ±0.03
b_0	0.675 ±0.05	0.99 ±0.05	1.00 ±0.05	0.730 ±0.05	1.00 ±0.05	1.00 ±0.05	0.70 ±0.20	0.94 ±0.05	0.91 ±0.06
h	0.050 ±0.010	0.415 ±0.010	0.400 ±0.010	0.004 ±0.003	1.00 ±0.01	1.00 ±0.01	0.052 ±0.017	0.080 ±0.010	0.040 ±0.010
b	0.880 ±0.01	0.820 ±0.01	0.830 ±0.01	0.775 ±0.01	0.645 ±0.01	0.650 ±0.01	0.905 ±0.01	0.865 ±0.01	0.865 ±0.01
c	0.680 ±0.01	0.640 ±0.01	0.630 ±0.01	0.950 ±0.01	0.890 ±0.01	0.895 ±0.05	0.620 ±0.01	0.725 ±0.01	0.705 ±0.01
q–bar	1 ± 1	1 ± 1	1 ± 1	3 ± 2	3 ± 2	3 ± 2	1 ± 1	1 ± 1	1 ± 1

w = single-scattering albedo, b_0 = opposition effect amplitude; *h* = opposition effect width; *b*, *c* = single particle scattering function parameters, q–bar = macroscopic roughness parameter